Stability of a stratified viscous shear flow in a tilted tube

Andrea Defina, Stefano Lanzoni, and Francesca M. Susin
Dipartimento di Ingegneria Idraulica, Marittima e Geotecnica, Università di Padova, Via Loredan 20, 35131 Padova, Italy

(Received 5 November 1997; accepted 15 October 1998)

The present investigation is concerned with the effects of viscosity on the stability of a bounded stratified shear flow with Prandtl number $\mathrm{Pr} \gg 1$. Theoretical results obtained from the solution of the Orr–Sommerfeld equation extended to stratified fluids are compared with experiments performed in a tilting tube filled with water and brine. Theoretical analysis shows that a complete stabilization of the flow field with respect to infinitesimal disturbances is attained, irrespective of the Richardson number J, as the Reynolds number Re decreases below 75. This damping action of viscosity is shown to appreciably reduce the critical Richardson number J_c with respect to the inviscid limit $J_c = 0.25$, even at moderately high Re. On the other hand, the destabilizing action enhanced by viscosity through the diffusion of momentum leads to a viscous mode of instability that may develop if J decreases below a threshold value. An extensive series of experiments has been carried out in a long tilting tube in order to verify theoretical results. The agreement between observations and theory is quite satisfactory. Kelvin–Helmholtz waves grow whenever theoretical unstable conditions are attained. The values of measured wavelengths well correspond to maximum growth rate wave numbers. The comparison between theoretical and experimental results also shows that acceleration plays a stabilizing action. © *1999 American Institute of Physics.*
[S1070-6631(99)00502-4]

I. INTRODUCTION

Considerable effort has been devoted during the last several decades to study the stability of stratified shear flows. In particular, the linear stability of inviscid, stably stratified, Boussinesq shear flow is now fairly well understood both for stepwise density profiles and for continuously stratified fluids.

The inviscid linear stability analysis of a generic velocity profile leads to the well-known Taylor–Goldstein equation (Miles[1] and Drazin and Howard[2]), which provides some general stability criteria (see Drazin and Reid[3]). The best known is probably the Miles–Howard theorem, which states that a sufficient condition for an inviscid stratified flow to be stable is that the local Richardson number exceeds 0.25 throughout the flow. Several mathematical and numerical studies of various density and velocity profiles have shown the existence of two basic physical mechanisms by which instability of a stratified fluid may be driven. The first one is the Kelvin–Helmholtz ($K-H$) instability, which may arise at the interface of two superposed layers of statically stable fluids flowing with different velocities. This kind of instability (for an extensive review see Thorpe[4]), which occurs provided that the local Richardson number of the flow falls below a critical value, is characterized by the growth of an initial disturbance to form a remarkably regular array of stationary billows with local mixing, and little or no propagation. The second mechanism of instability may arise provided that the density varies over a much smaller vertical scale than the velocity so that the density interface is embedded within the shear layer. This type of instability, usually called Holmboe (H) instability, is characterized by the formation of two trains of finite-amplitude waves that generate at the interface and propagate horizontally at the same speed but in opposite directions, inducing quite a small mixing (Holmboe,[5] Browand and Wang,[6] Browand and Winant,[7] Smyth *et al.*,[8] Smyth and Peltier,[9] Lawrence *et al.*,[10] and Baines and Mitsudera[11]).

Up to now much less is known about the stability of flows in which both viscosity and buoyancy, besides inertia forces, are important. It is known since Tollmien[12] that viscosity may play a non-negligible role in the stability of homogeneous parallel flows, since it dissipates energy of any disturbance and, therefore, is expected to stabilize the flow when a low enough value of the Reynolds number is achieved. On the other hand, a more complicated effect is related to the diffusion of momentum induced by viscosity that can lead to a conditionally destabilizing action (Benjamin[13]). Such a behavior is likely to be expected also in stratified shear flows.

The linear stability analysis developed by Hooper and Boyd[14] for the unbounded plane Couette flow of two fluids of different density and viscosity suggests that for a given value of the density ratio and in the short-wavelength limit an infinitesimal disturbance may amplify, decrease, or remain unchanged depending on the viscosity ratio. In particular, if the two fluids have the same viscosity and the surface tension at the interface is negligible, the flow results to be neutrally stable with respect to small short disturbances, irrespective of the density ratio. The analysis has been extended to all wave numbers and to the case of a bounded plane Couette flow by Renardy,[15] who showed that even a statically unstable stratification can be stabilized by a suitable arrangement of the viscous layers.

Yantsios and Higgins[16] studied numerically the linear stability of a plane Poiseuille flow of two superposed fluids of different viscosity and density. They found that depending on the density ratio, the viscosity ratio, and the ratio between the thickness of the layers, two different modes of instability may arise. At small Reynolds numbers the flow may be unstable to an ''interfacial mode'' (namely an instability mode that is enhanced by the presence of an interface), whereas, if the Reynolds number is sufficiently large, the flow can also be unstable to a shear mode of the Tollmien–Schlichting type. Although the latter result has been obtained by assuming equal densities in the two layers and neglecting the effects of both gravity and interfacial tension, a shear mode instability is likely to be expected also in a stratified flow driven by gravity.

Similar results are suggested by the linear stability analysis of thermally stratified shear flows with Prandtl number Pr close or equal to 1. Maslowe and Thompson[17] investigated numerically the stability of the laminar mixing region between two uniform unbounded streams. In particular, they solved the linear sixth-order equation, which can be derived for the disturbance amplitude function when the effect of both viscosity and heat conduction are accounted for. The resulting neutral stability curves suggest that the effects of viscosity and heat conduction do not greatly influence the stability of such a kind of flows. Nevertheless, these effects are found to be of primary importance within the critical layer for neutral and nearly neutral disturbances, and may lead to a significant distortion of the streamline pattern as the wave number α decreases.

On the other hand, a significant modification of the marginal stability curve is likely to be expected, due to viscosity effects, if the flow field is bounded by fixed surfaces. Gage and Reid[18] showed that the stability of thermally stratified plane Poiseuille flow is governed by three nondimensional parameters, namely, the Rayleigh number Ra, the Reynolds number Re, and the Richardson number Ri. They found that for $\mathrm{Pr}=1$ and $\mathrm{Ra}>1$ (i.e., when the density difference is destabilizing) two kinds of instability are possible. The first one is purely thermal in origin, arises at a value of the Rayleigh number that is independent of the shear and leads to steady convection in the form of longitudinal rolls whose axes are in the direction of the mean flow. The second one is of the Tollmien–Schlichting type. A sharp transition between the two modes is expected to occur at a small negative value of the Richardson number ($\mathrm{Ri}\approx -10^{-6}$); the smallness of this value emphasizes the dominant role of thermal instability for negative values of Ri. When the Richardson number is zero, the neutral stability curve shows that a critical value of the Reynolds number exists below which the flow is always stable. This critical value of Re increases as the Richardson number increases. However, the theory predicts that above $\mathrm{Ri}=0.0544$ the flow will be stable to small disturbances no matter how large is Re. Also, with any Richardson within the interval 0–0.0544 at large values of Re the instability is confined to a quite narrow range of wave numbers.

Gage[19] has extended the analysis to a velocity profile with an inflection point (i.e., Grohne's profile) showing that the above picture does not qualitatively change, although the numerical values are different.

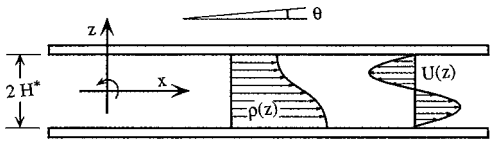

FIG. 1. Notations.

In this paper we focus our attention on flows in which the diffusion can be assumed to be negligible with respect to viscosity, so that $\mathrm{Pr}\gg 1$. In particular, we investigate both theoretically and experimentally the role of viscosity on the stability of a stratified bounded parallel shear flow that originates by tilting through a small angle a long rectangular tube, closed at the ends and filled with two layers of miscible fluids (namely clear and salt water) that are allowed to diffuse before tilting the tube. The paper is organized as follows. Section II is devoted to the mathematical formulation of the problem: basic flow relationships are derived and the main features of the linear stability analysis are discussed. Neutral marginal stability curves and growth rate curves, obtained by solving numerically the Orr–Sommerfeld equation extended to a stratified fluid, are shown. In Sec. III the experimental apparatus is described and the experimental results are discussed and compared with theoretical findings. Finally, Sec. IV is devoted to some conclusions.

II. FORMULATION OF THE PROBLEM

A. Formulation of the problem and basic flow

Let us consider the two-dimensional (2-D) stratified shear flow that arises when a long horizontal prismatic tube, closed at the ends, is suddenly tilted at an angle θ starting from rest (see Fig. 1). The change in density across the shear layer is assumed to be small enough for the usual Boussinesq approximation to hold. Moreover, it is assumed that diffusion is negligibly small when compared with viscosity (i.e., $\mathrm{Pr}\gg 1$). Therefore, the dimensionless governing equations can be written as

$$
\begin{aligned}
&u_{,t}+uu_{,x}+wu_{,z}=-p_{,x}+\frac{1}{\mathrm{Re}}\,(u_{,xx}+u_{,zz})-\frac{\rho\,\sin\,\theta}{\mathrm{Fr}^2},\\
&w_{,t}+uw_{,x}+ww_{,z}=-p_{,z}+\frac{1}{\mathrm{Re}}\,(w_{,xx}+w_{,zz})-\frac{\rho\,\cos\,\theta}{\mathrm{Fr}^2},\\
&u_{,x}+w_{,z}=0,\\
&\rho_{,t}+u\rho_{,x}+w\rho_{,z}=0,
\end{aligned}
\tag{1}
$$

where x,z are the longitudinal and the normal coordinates, t denotes time, u and w are the velocity components in the axial and normal direction, p is the pressure, ρ is the density, θ is the angle between the longitudinal axis and the horizontal direction, and Re and Fr are the Reynolds and Froude numbers, respectively. The variables have been made dimensionless in the form

$$(x,z)=\frac{(x^*,z^*)}{H^*};\quad (u,v,w)=\frac{(u^*,v^*,w^*)}{U_0^*};\quad t=\frac{t^*\cdot U_0^*}{H^*};$$
$$p=\frac{p^*}{\rho_0^* U_0^{*2}};\quad \rho=\frac{\rho^*}{\rho_0^*};\quad \mathrm{Re}=\frac{U_0^* H^*}{\nu};\quad \mathrm{Fr}=\frac{U_0^*}{\sqrt{gH^*}}, \tag{2}$$

where, denoting with a ''*'' superscript dimensional quantities, ν is the kinematic viscosity of the fluid, assumed constant, g is the gravitational acceleration, ρ_0^* is the mean density, and H^* and U_0^* are, respectively, half the depth of the tube and a reference velocity, which will be specified in the following. The choice of H^* as the characteristic length scale is strictly related to the form of velocity and density profiles herein considered, which, as it will emerge later on, both vary on half the depth of the tube.

In the following the parallel flow approximation is assumed to be valid and the dimensionless density profile is written as $\overline{\rho}(z)=1-\chi\beta(z)$, with χ defined so that $\beta_{,z}|_{z=0}=1$. The basic flow equations then read as

$$U_{,t}=-P_{,x}+\frac{1}{\mathrm{Re}}U_{,zz}-\frac{\sin\theta}{\mathrm{Fr}^2}+\frac{\chi\sin\theta}{\mathrm{Fr}^2}\beta(z);$$
$$P_{,z}=-\frac{\cos\theta}{\mathrm{Fr}^2}+\frac{\chi\cos\theta}{\mathrm{Fr}^2}\beta(z). \tag{3}$$

Equation (3b) states that $P_{,z}$ does not depend on x; as a consequence, $P_{,x}$ does not depend on z and the quantity $\xi_0=(-P_{,x}-\sin\theta/\mathrm{Fr}^2)$ on the right side of Eq. (3a) is, at most, a function of time.

Boundary conditions to be associated with Eqs. (3) express the physical requirement of no slip at the walls and, since the ends of the tube are closed, the requirement of no net flux across any plane normal to the flume,

$$U(z,t)|_{z=\pm1,t}=0;\quad \int_{-1}^{1}U(z,t)dz=0. \tag{4}$$

If $\beta(z)$ is an antisymmetric function [namely $\beta(z)=-\beta(-z)$], then condition (4b) implies

$$U(z,t)=-U(-z,t);\quad U(0,t)=0;\quad \xi_0=-P_{,x}-\frac{\sin\theta}{\mathrm{Fr}^2}=0, \tag{5}$$

and the basic flow equations (3) reduce to

$$U_{,t}=\frac{1}{\mathrm{Re}}U_{,zz}+\frac{\chi\sin\theta}{\mathrm{Fr}^2}\beta(z);$$
$$P_{,z}=-\frac{\cos\theta}{\mathrm{Fr}^2}+\frac{\chi\cos\theta}{\mathrm{Fr}^2}\beta(z). \tag{6}$$

The present investigations are concerned with the following density profile [Fig. 2(a)]:

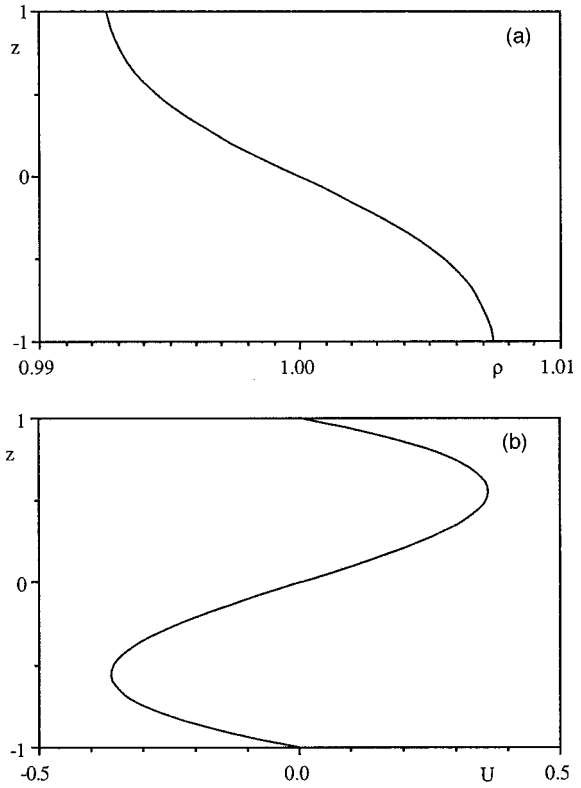

FIG. 2. Examples of the investigated density (a) and velocity (b) profiles.

$$\overline{\rho}(z)=1-\Delta\sum_{n=-\infty}^{+\infty}(-1)^n\cdot\mathrm{erf}[\sigma(z+2n)], \tag{7}$$

where Δ and σ are given constants and erf( ) is the error function. As discussed at the end of the present section and, more widely, in Sec. III, the choice of this particular density profile is related to the experimental conditions realized in order to check present theoretical results.

The equations (6) are thereby written in the form

$$U_{,t}=\frac{1}{\mathrm{Re}}U_{,zz}+\frac{\Delta\sin\theta}{\mathrm{Fr}^2}\sum_{n=-\infty}^{n=+\infty}(-1)^n\cdot\mathrm{erf}[\sigma(z+2n)],$$
$$P_{,z}=-\frac{\cos\theta}{\mathrm{Fr}^2}+\frac{\Delta\cos\theta}{\mathrm{Fr}^2}\sum_{n=-\infty}^{n=+\infty}(-1)^n\cdot\mathrm{erf}[\sigma(z+2n)]. \tag{8}$$

Even though the solution of the system (8) coupled with (4) could, in principle, be obtained in terms of the Laplace transform of the velocity (Thorpe[20,21]), a finite difference numerical approach has been adopted in order to evaluate the unsteady flow field characteristics. On the other hand, when considering steady flow conditions (i.e., $U_{,t}=0$), the following velocity profile is readily obtained [Fig. 2(b)]:

$$U(z)=\frac{\Sigma_{n=-\infty}^{+\infty}(-1)^n\left\{1/4[2(z+2n)^2+1/\sigma^2]\mathrm{erf}[\sigma(z+2n)]+\dfrac{z+2n}{2\sigma\sqrt{\pi}}e^{-[\sigma(z+2n)]^2}+\xi_1 z\right\}}{\Sigma_{n=-\infty}^{+\infty}(-1)^n\left(2n\cdot\mathrm{erf}(2n\sigma)+\dfrac{e^{-(2n\sigma)^2}}{\sigma\sqrt{\pi}}+\xi_1\right)}, \tag{9}$$

where the reference velocity, defined so that $U_{,z}|_{z=0}=1$ (Hazel[22]), is

$$U_0^*=\frac{gH^{*2}}{\nu}\,\Delta\,\sin\,\theta\sum_{n=-\infty}^{+\infty}(-1)^n \times\left(2n\cdot\mathrm{erf}(2\sigma n)+\frac{e^{-(2\sigma n)^2}}{\sigma\sqrt{\pi}}+\xi_1\right) \tag{10}$$

and

$$\xi_1=\sum_{n=-\infty}^{+\infty}(-1)^n\left(1/4[2(1+2n)^2+1/\sigma^2] \times\mathrm{erf}[\sigma(1+2n)]+\frac{1+2n}{2\sigma\sqrt{\pi}}\,e^{-[\sigma(1+2n)]^2}\right).$$

The uniform flow conditions characterized by the density distribution (7) and the velocity profile (9) will be set as the basis for the linear stability analysis developed in the next section.

Before we proceed any further, it is worth noticing that the density profile given by Eq. (7) comes from the solution of the Fick's diffusion equation, obtained by the method of superposition of image sources (Fischer *et al.*[23]) for the following case. We consider two superposed miscible fluids whose initially sharp interface is allowed to diffuse for a prescribed time τ_0^*. The two liquid layers have the same thickness H^*, are bounded by two rigid walls and are characterized by an initially stepwise density profile with upper and lower densities $\rho_1=1-\Delta$, $\rho_2=1+\Delta$, respectively.

The diffusion parameter σ, which appears in the solution, is related to the diffusion time τ_0^* by the relationship

$$\sigma=\frac{H^*}{2\sqrt{\kappa\tau_0^*}},$$

where κ is the molecular diffusivity ($\approx 1.4\times 10^{-9}$ m^2/s for the diffusion of salt in water).

In present theoretical and experimental investigations the choice of τ_0^* ($\approx$7200 s) and, as a consequence, of σ ($\approx$1.5), was related to the necessity of maintaining the maximum density difference close to its initial value 2Δ, and of satisfying the inequality $\tau_0^*\gg\tau_R^*$, τ_R^* ($\approx$15–80 s) being the duration of a given experiment. The latter requirement, implying that $\overline{\rho}(z,\tau_0^*+\tau_R^*)\approx\overline{\rho}(z,\tau_0^*)$, ensures that the diffusion process weakly affects the density distribution (and consequently the basic flow field) during each experiment. Finally, though the complete solution involves an infinite summation, nevertheless, it usually suffices to retain only a few terms ($n=\pm 10$ in our case) to obtain a quite good approximation of the actual density profile.

B. Linear theory

For a homogeneous fluid, Smyth and Peltier[9] applied Squire's[24] transformation to the linear stability of a steady nearly parallel viscous shear flow and demonstrated that the fastest growing mode of instability is always two dimensional, except in the instance that its growth rate not only increases with decreasing Reynolds number, but does so sufficiently fast.

The extension of Squire's theorem to the case of a stratified fluid has been first discussed by Yih.[25] A detailed analysis for special velocity and temperature profiles has been carried out by Koppel[26] and Gage and Reid[18] and, more recently, by Smyth *et al.*[8] and Smyth and Peltier.[9] In particular, Smyth and Peltier[9] demonstrated that the dominant mode of a stratified parallel shear flow is three dimensional if, and only if, the growth rate of the fastest growing two-dimensional disturbance increases sufficiently rapidly with decreasing Reynolds number and/or with increasing Richardson number. For the density and velocity profiles herein considered, no one of these two conditions is satisfied, since the results of the linear stability analysis developed in the following indicate that the growth rate of the fastest growing two-dimensional mode decreases with decreasing Reynolds number and with increasing Richardson number.

Therefore let us analyze the behavior of two-dimensional, infinitesimal disturbances, such that

$$[u,w,\rho,p]=[U(z),0,\overline{\rho}(z),P(z)] +\epsilon[\hat{u}(x,z,t),\hat{w}(x,z,t),\hat{\rho}(x,z,t),\hat{\rho}(x,z,t)], \tag{11}$$

with ϵ small (strictly infinitesimal) and $(\hat{u},\hat{w},\hat{\rho},\hat{p})=O(1)$.

Substituting (11) into the differential system (1) and performing linearization leads to a linear differential system subjected to homogeneous boundary conditions. A normal mode analysis can thus be pursued by assuming, due to the steady and nearly parallel character of the basic flow, that

$$(\hat{u},\hat{w},\hat{p},\hat{\rho})=[\hat{u}_0(z),\phi(z),\hat{p}_0(z),\hat{\rho}_0(z)]e^{i\alpha(x-ct)}, \tag{12}$$

where α is the wave number, $c=c_r+ic_i$ is the complex phase speed, and αc_i and αc_r are the growth rate and the angular frequency of disturbances, respectively. On substituting (12) into the linearized system and assuming a small inclination angle (i.e., $\cos\theta\cong 1$), after some algebra, the Orr–Sommerfeld equation for a stratified fluid is obtained,

$$\phi_{,zz}+\phi\left(-\frac{U_{,zz}}{U-c}-\alpha^2+\frac{JN^2}{(U-c)^2}\right) =\frac{1}{i\alpha\ \mathrm{Re}(U-c)}\,(\phi_{,zzzz}-2\alpha^2\phi_{,zz}+\alpha^4\phi), \tag{13}$$

where

$$JN^2=-\frac{1}{\mathrm{Fr}^2}\frac{\overline{\rho}_{,z}}{\overline{\rho}}, \tag{14}$$

$J^{1/2}N$ denoting the dimensionless Brunt–Väisälä frequency (Drazin and Reid[3]) and J being defined as the Richardson number evaluated in $z=0$,

$$J=-\frac{gH^*}{U_0^{*2}}\frac{1}{\overline{\rho}|_{z=0}}\frac{\overline{\rho}_{,z}|_{z=0}}{(U_{,z}|_{z=0})^2}=\frac{\chi gH^*}{U_0^{*2}}. \tag{15}$$

The Taylor–Goldstein equation, governing the stability of an inviscid fluid, is easily recovered from (13) in the limit of Re tending to infinity.

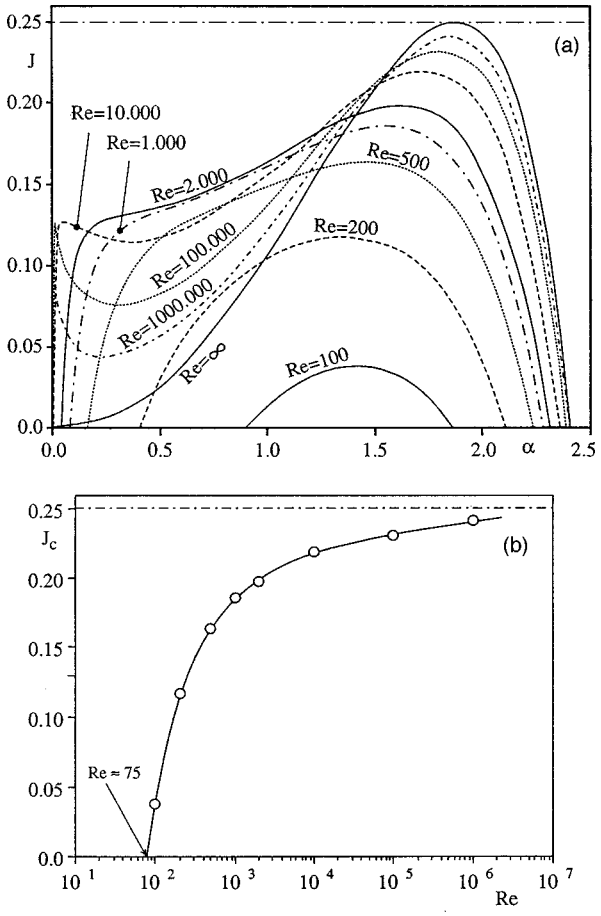

FIG. 3. (a) Theoretical neutral stability curves for different Reynolds numbers in the plane (α, J); (b) the theoretical critical Richardson number at the onset of K–H instability J_c plotted versus the Reynolds number.

The Orr–Sommerfeld equation, associated to the boundary conditions

$$\phi|_{z=\pm 1} = \phi_{,z}|_{z=\pm 1} = 0, \tag{16}$$

gives a dispersion relationship that can be formally written as

$$\mathfrak{T}(\alpha, c, J, \mathrm{Re}) = 0. \tag{17}$$

The problem of evaluating the eigenvalues associated with this relationship has been solved numerically using the method of complete orthonormalization proposed by Davey.[27] This is a simple and reliable method that may be used for solving two-point boundary-value problems without any restriction on the size of parameters such as the Reynolds number.

Neutral stability boundaries have been computed in the plane (α, J) at different Reynolds numbers for $\sigma = 1.5$ and are plotted in Fig. 3(a). Only stationary neutral stability curves exist since αc_r has been found to be always zero. The solution of the Taylor–Goldstein equation is recovered as Re approaches infinity, predicting an inviscid critical Richardson number J_c equal to 0.25 at the onset of $K-H$ instability. Because of viscosity, high wave numbers are stabilized and critical conditions (corresponding to the maxima of the curves at different Re) are shifted toward both smaller wave numbers and smaller J, as previously suggested by Thorpe.[22]

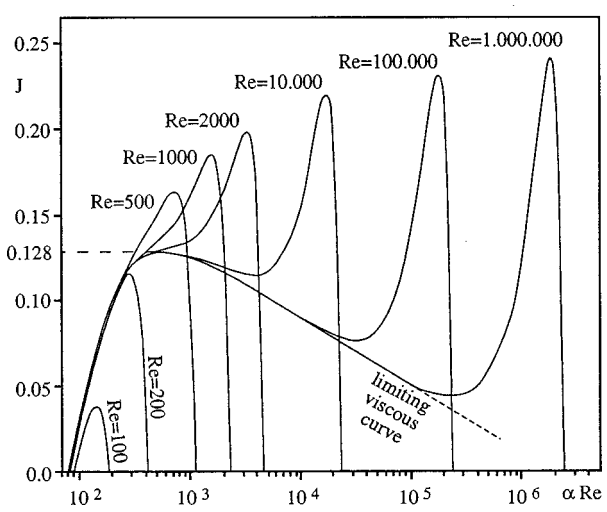

FIG. 4. Theoretical neutral stability curves for different Reynolds numbers in the plane (α Re, J).

The variation of the critical Richardson number J_c with Re is displayed in Fig. 3(b). An appreciable damping with respect to the inviscid limit 0.25 is evident, even at a moderately high Reynolds number, and complete stabilization, irrespective of J, is attained as Re decreases below 75.

A further effect of viscosity can be recognized in the range of low wave numbers. The region of instability for a viscous fluid turns out to be significatively enlarged, and for $\mathrm{Re} > \approx 3000$ the neutral stability curves are characterized by a relative maximum at $J \cong 0.128$ (hereafter referred to as J_{c1}), irrespective of Re.

This latter result is clearly displayed in Fig. 4, where neutral stability boundaries, plotted in the plane (α Re, J), exhibit a ''limiting viscous curve'' with a maximum for $J = J_{c1}$, from which the inviscid branches of neutral curves at different Re depart.

The existence of two different mechanisms of instability is better understood by analyzing the curves of neutral stability in the plane (α, Re). Three distinct behaviors can be recognized, depending on the value of J. For $0 \leqslant J < J_{c1}$, two neutral stability curves exist and a viscous mechanism of instability coexists with a K–H type of instability [Fig. 5(a)]. Two kinds of limits, in fact, are achieved as viscosity vanishes along the branches of the curves, depending on whether the inner and outer viscous layers remain well separated or not (see Drazin and Reid,[3] p. 166). The first class of limits, which are commonly referred to as inviscid limits, occurs along the upper branches of both the curves of neutral stability. The second class of limits, which can be referred to as viscous limits, occurs along the lower branches of the two marginal curves and is expected to be associated to a Tollmien–Schlichting mechanism of instability (Gage[19]). For J equal to J_{c1}, the lower branches of the two neutral curves join together when Re exceeds about 3000 [Fig. 5(b)]. Finally, for $J_{c1} < J < J_c$, a unique neutral curve exists, whose upper and lower branches correspond to the upper branches of the two neutral curves characterizing the previous range of J. In this case the viscous instability is completely stabilized and only $K-H$ instability is expected to arise [Fig. 5(b)].

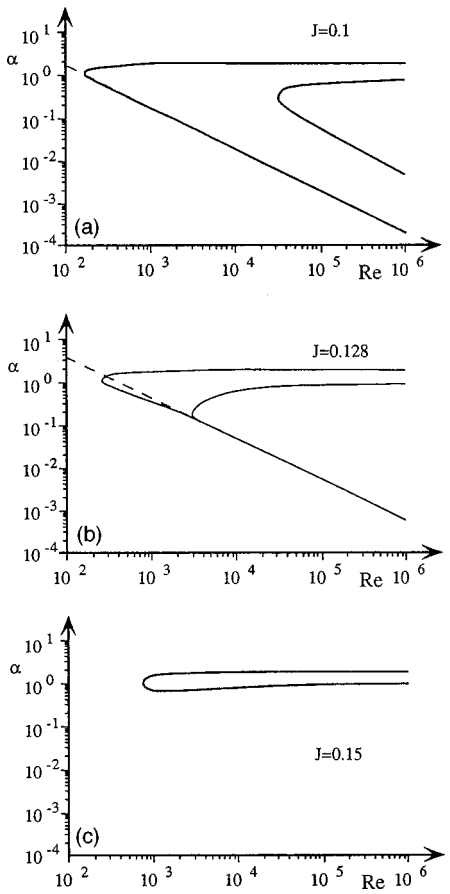

FIG. 5. Theoretical neutral stability curves in the plane (α,Re). (a) $0<J<J_{c1}$; (b) $J=J_{c1}$; (c) $J_{c1}<J<J_c$.

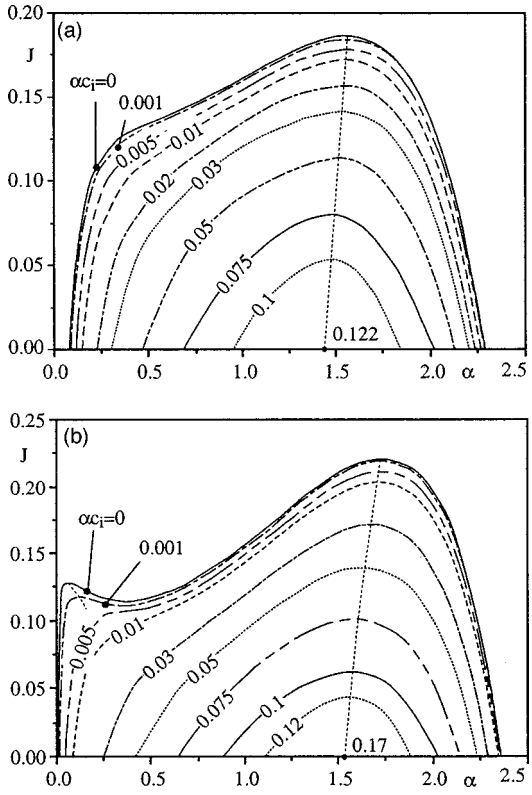

FIG. 6. Constant growth rate curves in the plane (α,J) for $\mathrm{Re}=10^3$ (a) and $\mathrm{Re}=10^4$ (b).

Although the different nature of density stratification and velocity profile herein considered, these results are qualitatively consistent with Gage's[19] theoretical findings. However, unlike the thermally stratified flows examined by Gage[19] it does not exist in the plane (α,Re) a limiting value of J above which neutral curves close up, bounding a region of instability.

In short, numerical calculations of the growth rate αc_i suggest that $K-H$ disturbances ultimately occur. As shown in Fig. 6, in fact, the curve of maximum αc_i lies in the region of $K-H$ instability, and for $0<J<J_{c1}$ the growth rates of low wave number disturbances (i.e., the viscous mode) are somewhat weaker than those for the $K-H$ modes.

III. EXPERIMENTS

A. Experimental apparatus

A suitably designed experimental apparatus has been used in order to check the validity of theoretical predictions, discussed in the previous section, concerning the effects of viscosity on the onset of instability in a stratified nearly parallel flow. As ingeniously conceived by Thorpe,[21] the occurrence of instability in such a shear flow can be investigated by tilting a horizontal rectangular tube filled with a stably stratified fluid mixture (Thorpe[22,28,29]). In present experiments, a perspex tube 377 cm long, 24 cm wide, and 2.22 ± 0.02 cm deep has been adopted. The tube can be pivoted about its median horizontal axis and, in order to avoid buckling, is supported on a C beam and stiffened with four steel bars.

The choice of the tube height and length is strictly related to the necessity of obtaining a flow field as close as possible to steady flow conditions before instability arises or the surges generating at the ends of the tube reach its middle section. Indeed the numerical solution of system (3) shows that in the tube herein adopted nearly self-similar velocity profiles are obtained after a time interval, ranging from about 15 to 20 s (see Fig. 7), which is usually lower than both the onset time of instability and the arrival time of the surges from the tube ends (the latter ranging from 30 to 80 s for the

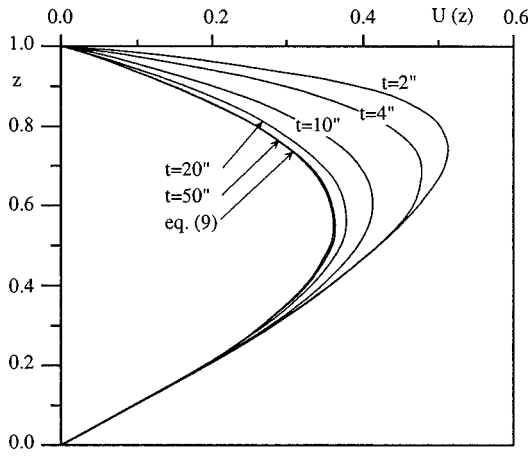

FIG. 7. Computed dimensionless velocity profiles at different times.

adopted values of $\Delta\rho/\rho$). Evidently, in such a thin tube upper and lower walls significantly influence the growth of disturbances to finite amplitudes and the transition to turbulence. However, we are concerned with the initiation of unstable motion close to onset, when the amplitude of disturbances is significantly smaller than the tube thickness and, consequently, upper and lower walls are likely to not affect the properties of instability.

The adopted miscible fluids were fresh water and a colored brine solution (for which $\mathrm{Pr}\approx 700$). Four different brine densities, namely $\rho=1005$, 1015, 1025, and 1035 kg/m^3, were used. Following the procedure outlined by Thorpe[21] the tube was filled from the bottom when its longest side was vertical in order to reduce mixing between the two fluids. When filled, the tube was carefully rotated from the vertical position until it was horizontal. As the two-fluid system had completely settled in the tube, diffusion between brine and water was allowed for a prescribed time τ_0^*. Typically, τ_0^* was approximately 2 h, thus implying $\sigma\approx 1.5$. Such a large value of τ_0^* was chosen in order to limit as much as possible the influence of the diffusion process during a given experiment and, also, to reduce uncertainties due to diffusion taking place during the rotation of the tube (Thorpe[22]).

At the time τ_0^* the tube was rapidly tilted by a small angle θ from its horizontal position; the tilting angle ranged from $-10°$ to $-1.6°$ and complete tilting was achieved in about 2 s.

The flow pattern in the middle section of the tube (hereafter referred to as the test section) was filmed by a CCD camera working at a speed of 25 frames per second. A mirror inclined at about 45° and placed below the tube ensured the plane view of the flow field. A stopwatch attached to the tube allowed, through the analysis of recorded images, to relate quite accurately the tube slope to time when tilting the tube and to evaluate the onset time of instability. The ''zero time'' was taken as the time when tilting began, while the onset time of instability, t_{exp}^*, was defined such as the instant at which the unstable mode began to be visible. In order to reduce the general uncertainties and subjectivity inherent to this t_{exp}^* evaluation procedure, measurements were performed by two different individuals and often repeated after a gap of some weeks, with minor differences in the results: maximum error in t_{exp}^* was found never to exceed 5%, being anyway smaller than 1 s.

The question of evaluating both Richardson and Reynolds numbers at the onset of instability deserves some discussion. Direct measurement of density and velocity profiles is quite a difficult task in the present experiments due to the small tube thickness. The requirement of avoiding, as far as possible, any artificial disturbance in the flow field would suggest the use of nonintrusive measuring techniques. On the other hand, the time scale of the phenomena is not long enough to allow laser Doppler anemometry measurements of velocity, but at one fixed point. Therefore, an indirect evaluation of density and velocity profiles (and consequently of Richardson and Reynolds numbers) is herein pursued by assuming that the density distribution in the tube is reasonably described by Eq. (5) and that instantaneous velocity profiles at the test section can be evaluated through numerical integration of Eqs. (3). The correspondence between computed and actual profiles was checked in an extensive series of preliminary runs by analyzing the displacement of a thin vertical line obtained by carefully injecting a small amount of dye in correspondence with the test section. After tilting the tube, the line deformed according to the total displacement of water, which strongly depends upon actual density and velocity profiles and, hence, can be profitably used to evaluate the effectiveness of the present approach. Indeed, the comparison between computed and measured maximum displacement of the tracer at different times appears to be satisfactory, as shown in Fig. 8(a). Many more difficulties were met when comparing tracer profiles at different times because of the strong refraction effects acting at the diffuse interface. Compression and widening of the image just below and above the interface, respectively, produced a remarkably distorted picture of the tracer profile. A correction of recorded tracer profiles based on the deformation of a ruler located behind the diffuse interface was adopted (see Mowbray[30]). The agreement between observed and computed tracer profiles shown in Fig. 8(b) appears to be satisfactory.

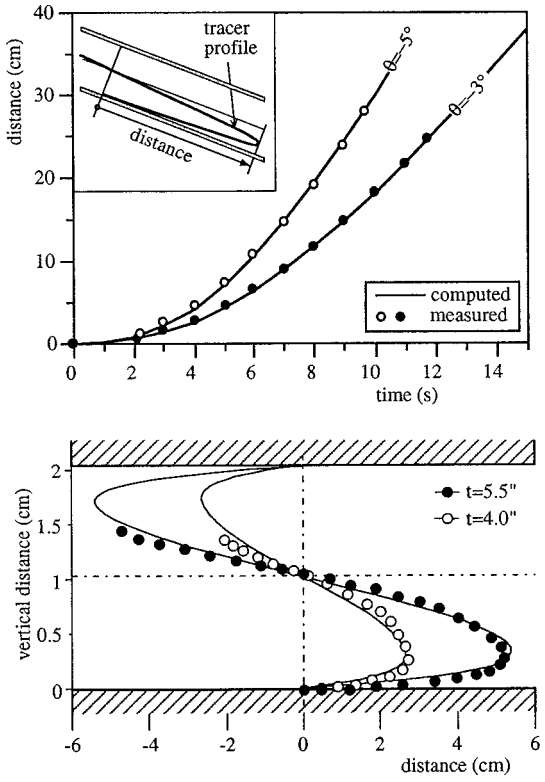

FIG. 8. (a) A comparison between measured and computed maximum tracer longitudinal displacement; (b) a comparison between measured and computed tracer profiles at $\theta=-3°$. Here $\Delta\rho/\rho=0.025$.

The above findings suggest that both Reynolds and Richardson numbers can be confidently estimated on the basis of computed values of density and velocity. The influence of possible errors in t_{exp}^* on J and Re values was estimated, assuming a 5% error in t_{exp}^*, as previously reported (Fig. 9). According to numerical calculations, a 4.5% error in Re and a 8.5% error in J are expected at the most, i.e., when insta-

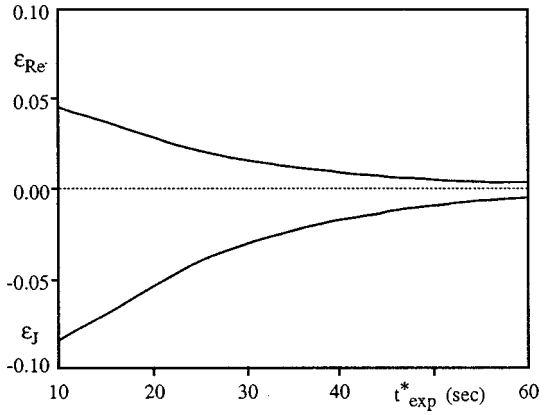

FIG. 9. Errors in Reynolds and Richardson numbers for a 5% error in t^*_{exp}.

bilities are being observed at about $t^*_{exp}=10$ s; these errors decrease quite rapidly as t^*_{exp} increases.

Figure 10 shows the typical time evolution, during a given run, of Reynolds and Richardson numbers, and of the critical Richardson number for the onset of instability J_c predicted by the linear stability analysis developed in Sec. II B. The plot allows us to determine the time t^*_c at which J equals J_c; shortly after t^*_c some disturbances are expected to grow, provided that flow unsteadiness effects can be neglected, as will be discussed in the next section.

B. Experimental results

As stated in Sec. III A, about 15–20 s after tilting the tube velocity profiles become nearly self-similar. Furthermore, shortly after $t^*=t^*_c$ the rate of change of the accelerating flow $U_{,t}/U$ has been found to be much smaller than the growth rate αc_i of disturbances, thus suggesting that the quasisteady approximation (Thorpe[22]) can be assumed. In other words, the growth rate of an unstable disturbance at a given time is supposed to be the same as for a steady flow, characterized by the same distribution of density and velocity of the accelerating flow at that instant in time. On the basis of this assumption present experimental results are compared with the theoretical findings discussed in Sec. II B concerning uniform flow conditions.

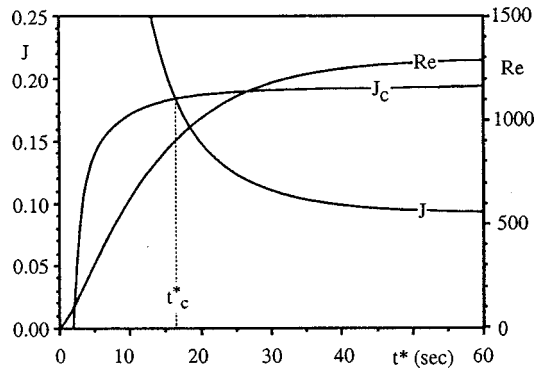

FIG. 10. The evolution of Re(t), $J(t)$, $J_c(t)$ in a given run. Here $\Delta\rho/\rho=0.015$; $\theta=-3.5°$.

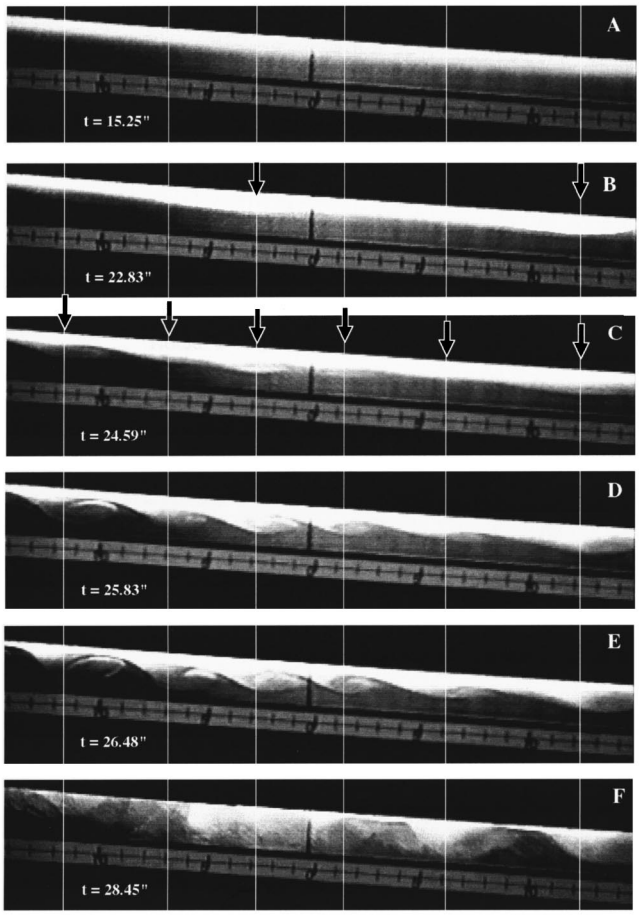

FIG. 11. Instabilities developing in the tilted tube. Here $\Delta\rho/\rho=0.015$; $\theta=-4°$. A few seconds after tilting the tube, over the initially unperturbed interface (A) a small-amplitude long wave appears (B). Soon after, two-dimensional shorter waves develop at the interface (C–E) and, finally, disrupt into turbulence (F). Arrows mark the positions of long wave troughs (frame B) and of short wave troughs (frame C).

The 37 experimental runs carried out are grouped in the following classes:

runs in which no instability were detected (hereafter referred to as STBL);

runs in which long waves were observed to grow slightly before the onset of shorter Kelvin–Helmholtz waves (hereafter referred to as LW-KH);

runs in which only a Kelvin–Helmholtz instability developed (hereafter referred to as KH).

Before discussing experimental results, a qualitative description of the evolution of the observed instabilities is given in Fig. 11. In LW-KH experiments, a few seconds after tilting the tube, long, stationary, two-dimensional waves generated (frame B) with a characteristic wavelength λ^*_L of about 14 cm ($\lambda^*_L/H^*\sim$ ''12–16''). Soon after, a very regular array of shorter two-dimensional and stationary waves suddenly developed all along the tube (frame C). These waves grew almost simultaneously until they rolled up (frames D and E) and, finally, disrupted into turbulence (frame F). Sometimes disruption occurred before complete rolling, as the wave crests reached the upper wall of the tube. In KH runs only the instability evolution described in frames

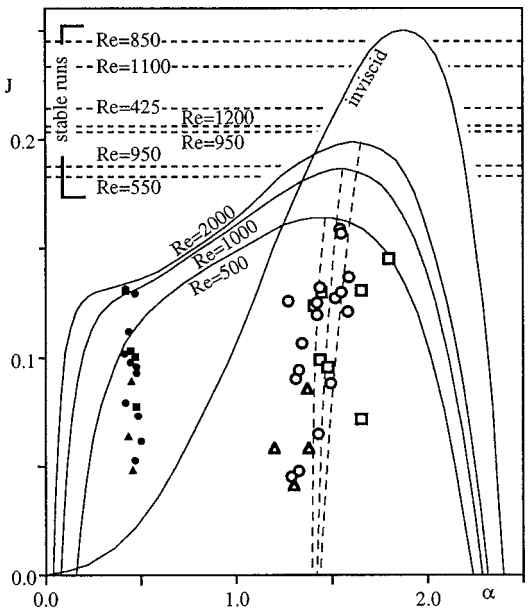

FIG. 12. Experimental data (α,J) observed at the onset of instability compared with the theoretical neutral stability curves. Open and full symbols denote short and long wave data, respectively. □■, 500<Re<1000; ○●, 1000<Re<20000; △▲, Re>2000.

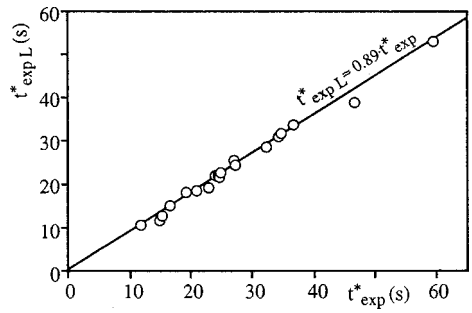

FIG. 13. The onset time of the observed long waves $t^*_{\exp L}$ plotted against the onset time of Kelvin–Helmholtz instability $t^*_{\exp}$.

C–F was observed. The wavelength of shorter waves λ_s^* ranged between 4.3–5.8 cm. Both λ_s^* and λ_L^* did not change appreciably during the growth; for this reason they were measured from the recorded images a few moments after the early stage of the growth of the disturbances. The wave number of short waves was observed to be approximately the same also in the absence of long waves, i.e., in KH runs.

The two-dimensional nature of growing disturbances typical of the early stage of instability (frames A–D of Fig. 11) has been ascertained analyzing the plane view of the flow field reflected by the mirror placed below the tube. Sidewall effects such as those pointed out by previous experimental investigations (Thorpe[4]) have been observed to occasionally affect the flow structure only in the advanced stage of billow growth when the wave amplitude was considerably large.

It is also worth pointing out that during the time elapsed between the appearance of the long and the short waves, Re and J changed, on average, only about 3% and 6%, respectively, thus suggesting that the two instabilities develop in quite similar basic flow fields.

A comprehensive view of the experimental results is shown in Fig. 12, where the observed wave number α of both long and short waves are plotted versus the Richardson number. All data lie in the region of instability below the theoretical neutral stability curve corresponding to the Reynolds number evaluated at the appearance of disturbances. Data corresponding to short waves arrange, with acceptable scatter, around the line of the maximum growth rate predicted by the linear theory, the scatter possibly being related to the relatively small number of waves (6–8) used to compute the average wavelength. Points referring to long waves lie in the region of the (α,J) plane, where, according to the linear theory, the destabilizing action enhanced by viscosity through the diffusion of momentum is likely to develop, at $\alpha\approx\alpha_L\approx 0.5$.

It is important to notice that in all KH runs (i.e., in the absence of long waves) J was greater than the theoretical critical value predicted for $\alpha\approx\alpha_L$. This circumstance suggests that in these runs J was such as to inhibit viscous instability, as it can be inferred by the following argument. Let us consider Fig. 13, where, on the basis of LW-KH runs, the onset time of long waves $t^*_{\exp L}$ is plotted against the onset time of short waves $t^*_{\exp}$. A fairly good linear correlation was empirically derived, yielding $t^*_{\exp L}\cong 0.89 t^*_{\exp}$ $(R^2=0.991)$. This correlation allows us to estimate the time $\hat{t}_L^*$ at which long waves would have had to appear in KH runs and, accordingly, to calculate the related $\mathrm{Re}(\hat{t}_L^*)$ and $J(\hat{t}_L^*)$. The points specified by $J(\hat{t}_L^*)$, $\mathrm{Re}(\hat{t}_L^*)$, and $\hat{\alpha}_L\approx 0.5$ (i.e., by assuming that the wave number would have fallen within the range typically selected by the observed long waves) all lie outside the instability region.

Although theoretical conditions for both amplification and damping of viscous modes of instability appear to be satisfied, nevertheless, the occurrence of long waves prior to the formation of $K-H$ waves is an unexpected result that cannot be fully understood in the light of the stability analysis herein performed. Linear theory, in fact, shows that shorter waves with $\alpha\approx 1.5$ are characterized by the highest growth rate, thus suggesting that this wave number is the one selected by the instability mechanism during experiments. Equally surprising is the sharply defined preferred wavelength exhibited by the long waves $(\alpha_L\approx 0.5)$, whereas the growth rate curves shown in Fig. 6 indicate no such preference. The tube was then disassembled and accurately checked, but no sources of noise able to bias instability in favor of longer wavelengths was found.

Figure 12 also shows the experimental values of Re and J achieved at the end of STBL runs, which were carried out in order to verify theoretical conditions for the decaying of disturbances. In these experiments small tilting angles were adopted such that J never decreased below the theoretical critical value J_c; also, numerical calculation showed that acceleration rapidly became negligibly small. As expected, stable conditions were always observed to persist until the end of each run (i.e., when the surges penetrating from the ends of the tube reached the test section). The fact that in all STBL experiments, shortly after tilting the tube, J decreased

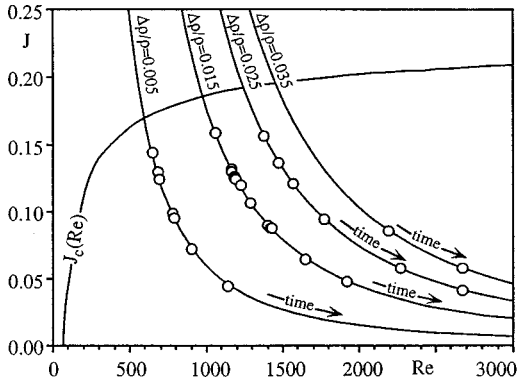

FIG. 14. Trajectories corresponding to the time evolution of the experimental basic flow plotted in the (Re, J) plane for different $\Delta\rho/\rho$ along with the theoretical neutral curve J_c(Re) and the experimental critical points ($\mathrm{Re}_{\mathrm{exp}}$, J_{exp}) denoted with open circles.

below the inviscid limit 0.25 confirms the stabilizing action of viscosity discussed in Sec. II B.

A comparison between experimental and theoretical critical conditions also pointed out that in many runs $J_{\mathrm{exp}} = J(t^*_{\mathrm{exp}})$ was significantly smaller than J_c. This is recovered in Fig. 14, where, for different values of $\Delta\rho/\rho$, trajectories corresponding to the time evolution of the basic flow during a given run are plotted in the plane (Re, J) along with the neutral curve J_c(Re) and the experimental critical points ($\mathrm{Re}_{\mathrm{exp}}$, J_{exp}) [with $\mathrm{Re}_{\mathrm{exp}}=\mathrm{Re}(t^*_{\mathrm{exp}})$]. The above discrepancy can be ascribed to the flow unsteadiness. In Fig. 15 the ratio of the experimental to the theoretical critical Richardson number J_{exp}/J_c is plotted versus the dimensionless acceleration $a=(H^*/U_0^{*2})dU_0^*/dt^*$. It clearly appears that J_{exp}/J_c decreases as acceleration increases and approaches unity as acceleration tends to zero.

In order to elucidate the stabilizing effect of acceleration, an additional set of experiments was performed. In these experiments, hereafter referred to as STD, the tube was tilted twice during each run such as to obtain nearly uniform flow conditions. Namely, the tube was initially tilted at an angle θ and the flow was allowed to develop until an almost self-similar velocity profile established with a selected value U_s^* of the reference velocity (the related Reynolds and Richardson numbers being denoted with Re_s and J_s, respectively). At this time, the tube was rapidly tilted back at the angle $\theta_s<\theta$, related to U_s^* through Eq. (10). Since the tilting

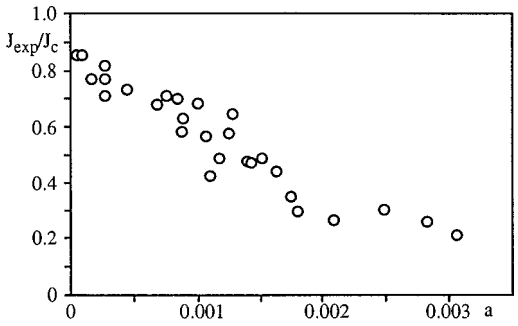

FIG. 15. Ratio of the experimental to the theoretical critical Richardson numbers J_{exp}/J_c plotted against dimensionless acceleration a.

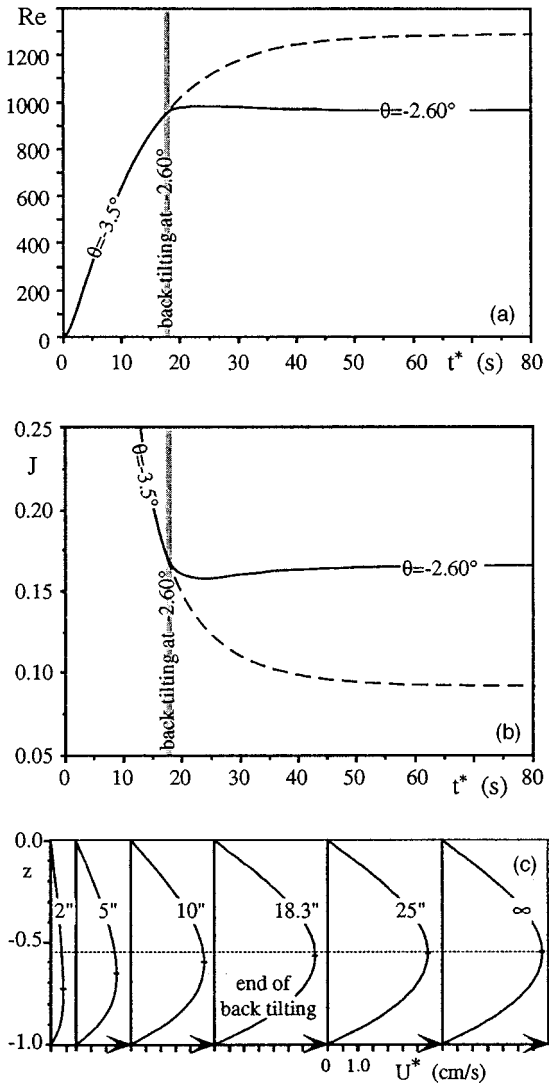

FIG. 16. The time evolution of Reynolds (a) and Richardson (b) numbers and dimensional velocity profiles at different times (c) in a STD run. Here $\Delta\rho/\rho=0.015$; $\theta=-3.5°$; $\theta_s=-2.6°$.

was not instantaneous and as a consequence of fluid inertia, the chosen uniform conditions were achieved after a time lag in which acceleration rapidly decayed to zero. An example of the behavior of Reynolds and Richardson numbers during a run and time evolution of velocity profiles are plotted in Fig. 16.

The outlined procedure allowed to ''freeze'' the flow when the Richardson number J_s lied between J_c(Re) and the critical value $J_{\mathrm{exp}}(\mathrm{Re}_{\mathrm{exp}})$ found in previous experiments affected by acceleration (see Fig. 14). All values of J_s experimentally reproduced and the related values of θ_s (θ and $\Delta\rho/\rho$ always being equal to $-3.5°$ and 0.015, respectively) are shown in Fig. 17, where J is plotted as a function of time for the different experimental conditions. Notice that in these experiments it has been possible to achieve values of J very close to the theoretical critical value J_c (namely $J_s=0.978\cdot J_c$ for $\theta_s=-2.50°$ and $J_s=0.994\cdot J_c$ for $\theta_s=-2.48°$). As theoretically predicted, K–H instability was found to arise in all runs shortly after the tube was tilted back at θ_s. Also,

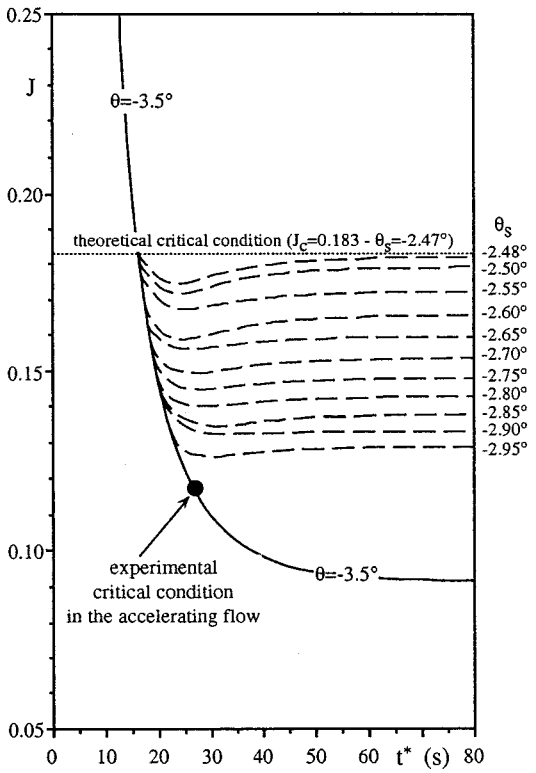

FIG. 17. The Richardson number plotted against time for the various back-tilting angles adopted in STD runs with $\Delta\rho/\rho=0.015$; $\theta=-3.5°$; θ_s ranging from $-2.95°$ to $-2.48°$.

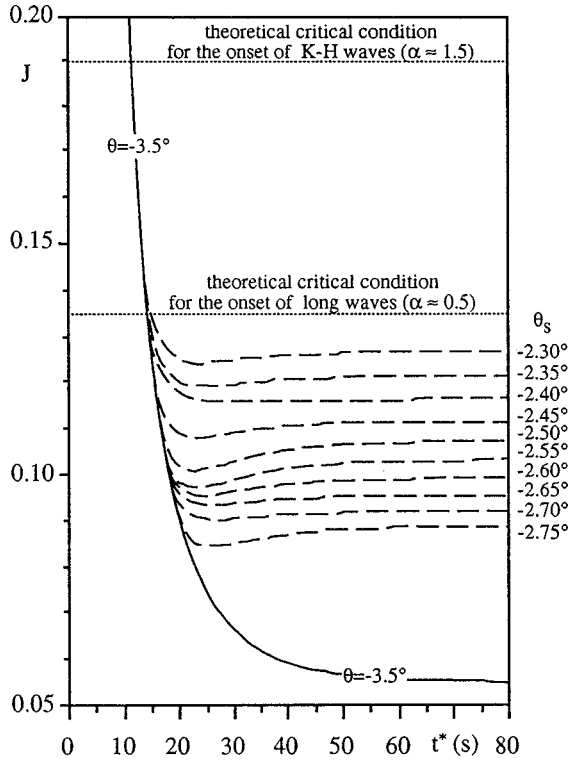

FIG. 18. The Richardson number plotted against time for the various back-tilting angles adopted in STD runs with $\Delta\rho/\rho=0.025$; $\theta=-3.5°$; θ_s ranging from $-2.75°$ to $-2.30°$.

wave numbers of the observed disturbances were in good agreement with theoretical critical values located close to the maximum growth rate curves.

Some additional STD runs have also been performed with $\theta=-3.5°$, $\Delta\rho/\rho=0.025$ such that the Richardson number J_s was low enough to allow, according to steady stability analysis, the growth of both $K-H$ waves ($\alpha\approx1.5$) and disturbances with $\alpha\approx0.5\approx\alpha_L$ (Fig. 18): in all these runs, long waves were never detected while short waves were always observed to grow.

This result suggests that acceleration might have a non-negligible role in the selection of early growing wave numbers (i.e., in the formation of long waves before Kelvin Helmholtz waves in LW-KH runs). In particular, it might be conjectured that acceleration acts more effectively in stabilizing higher wave numbers and modifies the shape of neutral stability curves so that long waves are likely to grow before $K-H$ waves. As acceleration progressively decays during a given LW-KH run, the neutral curves tend to approach the ones calculated for steady flow conditions leading, ultimately, to the prevalence of the $K-H$ mode of instability experimentally observed in unsteady runs.

IV. CONCLUSIONS

In this work the influence of viscosity on the stability of a stratified shear flow has been examined both theoretically and experimentally. The theoretical analysis was focused on the steady velocity profiles that develop in a closed tilted tube filled with fresh water and brine. A diffused interface density profile has been investigated. The neutral marginal stability curves computed at different Reynolds numbers solving the Orr–Sommerfeld equation have been compared with the one calculated for an inviscid fluid based on the Taylor–Goldstein equation. According to theoretical analysis, the effects of viscosity for the studied shear flow can be summarized as follows.

(i) The critical Richardson number J_c at the onset of instability decreases with Reynolds number until complete stabilization is achieved for $\mathrm{Re}<75$, no matter how small J is. Nevertheless, the reduction of J_c induced by the damping action of viscosity is already appreciable at moderately high Reynolds numbers (e.g., at $\mathrm{Re}=2000$ a reduction of J_c by approximately 20% is attained).

(ii) At low wave numbers the unstable region expands toward higher Richardson numbers. A second relative maximum appears due to viscosity effects when the Reynolds number exceeds approximately the value of 3000. This maximum is characterized by a single threshold value of the Richardson number $J_{c1}=0.128$, above which the weak instability of viscous origin is completely stabilized.

(iii) A ''limiting viscous curve'' can be recognized from which, eventually, the inviscid branches of neutral stability curves depart.

(iv) The maximum growth rates of the disturbances are located near the absolute maximum of the inviscid branches, which suggests that a $K-H$ instability will ultimately occur.

Theoretical findings were confirmed in both weakly accelerating flow and steady flow experiments. No instabilities were, in fact, observed to grow when J remained above its theoretical critical value while K–H waves always appeared whenever theoretical unstable conditions were attained. Also the stabilizing effect related to the local flow acceleration was recognized and, though indirectly, confirmed.

The observed growth of stationary long waves ($\alpha \approx 0.5$) some instants before the onset of K–H instability ($\alpha \approx 1.5$) in weakly accelerating flow experiments was an unexpected result, being not predicted nor suggested by the linear theory. On the contrary, in steady flow experiments long waves were never detected, thus suggesting that flow unsteadiness might be responsible for the appearance of long waves.

ACKNOWLEDGMENTS

The authors would like to acknowledge Professor L. D'Alpaos for his friendly encouragement and fruitful discussions. The authors are also indebted to the referees for their useful comments and suggestions.

[1] J. W. Miles, ''On the stability of heterogeneous shear flows,'' J. Fluid Mech. **10**, 496 (1961).
[2] P. G. Drazin and L. N. Howard, ''Hydrodynamic stability of parallel flow of inviscid fluids,'' Adv. Appl. Mech. **9**, 1 (1966).
[3] P. G. Drazin and W. H. Reid, *Hydrodynamic Stability* (Cambridge University Press, Cambridge, 1981).
[4] S. A. Thorpe, ''Transitional phenomena and the development of turbulence in stratified fluids: a review,'' J. Geophys. Res. **92**, 5231 (1987).
[5] J. Holmboe, ''On the behavior of symmetric waves in stratified shear layers,'' Geofys. Publ. **24**, 67 (1962).
[6] F. K. Browand and Y. H. Wang, ''An experiment on the growth of small disturbances at the interface between two streams of different densities and velocities,'' *International Symposium on Stratified Flows*, Novosibirsk, 1972 (ASCE, New York, 1972), p. 491.
[7] F. K. Browand and C. D. Winant, ''Laboratory observations of shear layer instability in a stratified fluid,'' Boundary-Layer Meteorol. **5**, 67 (1973).
[8] W. D. Smyth, G. P. Klaassen, and W. R. Peltier, ''Finite amplitude Holmboe waves,'' Geophys. Astrophys. Fluid Dyn. **43**, 181 (1988).
[9] W. D. Smyth and W. R. Peltier, ''Three-dimensional primary instabilities of a stratified, dissipative, parallel flow,'' Geophys. Astrophys. Fluid Dyn. **52**, 249 (1990).
[10] G. A. Lawrence, F. K. Browand, and L. G. Redekopp, ''The stability of a sheared density interface,'' Phys. Fluids A **10**, 2360 (1991).
[11] P. G. Baines and H. Mitsudera, ''On the mechanism of shear flow instabilities,'' J. Fluid Mech. **276**, 327 (1994).
[12] W. Tollmien, ''Über die enststehung der turbulenz,'' Nacht. Ges. Wiss. Göttingen, Math.-phys. Kl., 1929; translated as ''The production of turbulence,'' Tech. Memor. Nat. Adv. Comm. Aero., Washington, DC, 1931, p. 609
[13] K. S. Benjamin, ''The threefold classification of unstable disturbances in flexible surfaces bounding inviscid flows,'' J. Fluid Mech. **16**, 436 (1963).
[14] A. P. Hooper and W. G. C. Boyd, ''Shear-flow instability at the interface between two viscous fluids,'' J. Fluid Mech. **128**, 507 (1983).
[15] Y. Renardy, ''Instability at the interface between two shearing fluids in a channel,'' Phys. Fluids **28**, 3441 (1985).
[16] S. G. Yiantsios and B. G. Higgins, ''Linear stability of plane Poiseuille flow of two superposed fluids,'' Phys. Fluids **31**, 3225 (1988).
[17] S. A. Maslowe and J. M. Thompson, ''Stability of a stratified free shear layer,'' Phys. Fluids **14**, 453 (1971).
[18] K. S. Gage and W. H. Reid, ''The stability of thermally stratified plane Poiseuille flow,'' J. Fluid Mech. **33**, 21 (1968).
[19] K. S. Gage, ''The effect of stable thermal stratification on the stability of viscous parallel flow,'' J. Fluid Mech. **47**, 1 (1971).
[20] P. Hazel, ''Numerical studies of the stability of inviscid stratified shear flows,'' J. Fluid Mech. **51**, 39 (1972).
[21] S. A. Thorpe, ''A method of producing a shear flow in a stratified fluid,'' J. Fluid Mech. **32**, 693 (1968).
[22] S. A. Thorpe, ''Experiments on the instability of stratified shear flows: miscible fluids,'' J. Fluid Mech. **46**, 299 (1971).
[23] H. B. Fischer, E. J. List, R. C. Y. Koh, J. Imberger, and N. H. Brooks, *Mixing in Inland and Coastal Waters* (Academic, New York, 1979).
[24] H. B. Squire, ''On the stability of three-dimensional disturbances of viscous flow between parallel walls,'' Proc. R. Soc. London, Ser. A **142**, 621 (1933).
[25] C. S. Yih, ''Stability of two-dimensional parallel flows for three dimensional disturbances,'' Q. Appl. Math. **12**, 434 (1955).
[26] D. Koppel, ''On the stability of flow of thermally stratified fluid under the action of gravity,'' J. Math. Phys. **5**, 963 (1964).
[27] A. Davey, ''A simple numerical method for solving Orr–Sommerfeld problems,'' Q. J. Mech. Appl. Math. **XXVI**, 401 (1973).
[28] S. A. Thorpe, ''Turbulence in stably stratified fluids: a review of laboratory experiments,'' Boundary-Layer Meteorol. **5**, 95 (1973).
[29] S. A. Thorpe, ''Experiments on instability and turbulence in a stratified shear flow,'' J. Fluid Mech. **61**, 731 (1973).
[30] D. E. Mowbray, ''The use of schlieren and shadowgraph techniques in the study of flow patterns in density stratified liquids,'' J. Fluid Mech. **27**, 595 (1967).